January 2010

A method for delivering spatio-temporally focused energy to a dynamically adjustable target along a waveguiding structure

J. B. Laflen

T. M. Talavage

Laflen, J. B. and Talavage, T. M., "A method for delivering spatio-temporally focused energy to a dynamically adjustable target along a waveguiding structure" (2010). *Department of Electrical and Computer Engineering Faculty Publications.* Paper 46.
http://dx.doi.org/http://dx.doi.org/10.1109/TSP.2009.2033310

A Method for Delivering Spatio-Temporally Focused Energy to a Dynamically Adjustable Target Along a Waveguiding Structure

J. Brandon Laflen, *Member, IEEE*, and Thomas M. Talavage, *Member, IEEE*

***Abstract*—It is possible to exploit the frequency-dependent velocity dispersion inherent to waveguiding structures to deliver spatio-temporally focused energy to a spatial target anywhere along the longitudinal extent of a waveguide. Such focusing of energy may have application to technologies as varied as nerve stimulation or chemical etching. A waveguide signal that effects this focused energy is conceptualized and derived. The spatial location of the target acted upon by the waveguide signal is demonstrated to be dynamically adjustable with a linear filtering step. Optimal parameters for waveguide signal generation are derived in the general case, allowing for application to a cross section of homogeneous waveguides. Performance is also considered in non-ideal, absorptive media. Numerical simulations are presented that indicate agreement with analytic results, and an evaluation of possible reduction to practice is presented.**

***Index Terms*—Energy conversion, filters, focusing, waveguides.**

I. Introduction

A WIDE range of applications use spatio-temporally focused energy as a catalyst for a desired system activation. Two examples of this range are etching with electrically-activated chemicals and stimulation of electrically excitable neural populations with a sensory prosthetic. Although the applications vary in scale and modality, control over the location and concentration of the focused energy is critical to optimal performance, affecting product miniaturization, speed, and resolution. In practice, a variety of methods deliver focused energy to spatial targets, including electromechanical positioning, optical lenses, and discrete electrode arrays.

One potential method for spatially focusing energy develops from the frequency-dependent velocity dispersion inherent to a large class of waveguiding structures. While many waveguiding structures exhibit dispersion, this paper will focus on a class of idealized structures with a single mode of excitation that is governed by the propagation relation

$$\beta(\omega) = \frac{1}{\nu_{\mathrm{M}}}\sqrt{\omega^2 - \omega_{\mathrm{C}}^2} \tag{1}$$

where ω_{C} is the intrinsic cutoff frequency of the waveguide, and ν_{M} is the theoretical maximum propagation velocity within the structure [1], [2]. The propagation relation is incorporated into the waveguide transfer function as a frequency-dependent phase-delay for waves propagating a distance z

$$H(\omega, z) = e^{-\jmath\beta(\omega)z}. \tag{2}$$

The propagation relation also leads to the frequency-dependent group velocity ν_{g}, associated with the center frequency of a given frequency-band ω_{g}

$$\nu_{\mathrm{g}} \stackrel{\mathrm{def}}{=} \frac{d\omega}{d\beta} = \nu_{\mathrm{M}}\sqrt{1 - \left(\frac{\omega_{\mathrm{C}}}{\omega_{\mathrm{g}}}\right)^2}. \tag{3}$$

Frequency-bands of wave energies, centered at different frequencies above cutoff ($\omega_{\mathrm{g}} > \omega_{\mathrm{C}}$), propagate along the waveguide at differing group velocities dictated by (3).

It is possible to exploit the natural dispersion of waveguiding structures, represented by (2), to produce a signal that spatially decays in amplitude from its maximum at a target location within the waveguide. Formally, we seek a signal $i(t)$ with Fourier spectrum $I(\omega) = \mathcal{F}\{i(t)\}$, and with peak amplitude $\sigma(z) = \max_t \mathcal{F}^{-1}\{I(\omega) \cdot H(\omega, z)\}$, such that $\sigma(z)/\sigma(z_T)$ is minimized $\forall\,|z - z_T| > 0$; here z_T represents the spatial target along the waveguide. This is an open-ended optimization problem that is related to efforts in other areas. For example, this problem is related to sensor network optimization problems [3], [4], where the "sensor input" is the spatially-distributed field intensity (each sensor represents a different location along the guide) and the sensor and channel transmission are the waveguide transfer function. Under this paradigm, the input signal is free, not the fusion algorithm, and the optimization criterion is as specified above. It is also desirable that the performance of this signal be robust to low levels of added system noise, so the posed inverse network problem is also related to blind separation problems [5]. Finally, it is noteworthy that in real applications (e.g., implantable prostheses) the waveguide transfer function may be parameterized, where the parameters

Manuscript received August 29, 2007; accepted August 17, 2009. First published September 29, 2009; current version published February 10, 2010. The associate editor coordinating the review of this manuscript and approving it for publication was Dr. Brian M. Sadler.

J. B. Laflen is with the Departments of Otolaryngology and Physiology & Neuroscience, School of Medicine, and the Courant Institute of Mathematical Sciences, New York University, New York, NY 10016 USA (e-mail: j.brandon.laflen@ieee.org).

T. M. Talavage is with the School of Electrical and Computer Engineering and the Weldon School of Biomedical Engineering, Purdue University, West Lafayette, IN 47907 USA (e-mail: tmt@purdue.edu).

Digital Object Identifier 10.1109/TSP.2009.2033310

must be estimated in noise for a large number of specific instances (e.g., individual variance across implanted embodiments). In this case, the optimal input signal must be derived in terms of the noisy estimates. As such, this optimization problem also intersects with those related to noisy parameter estimation [6]–[9].

One possible solution to the general problem uses frequency-dependent group velocity to construct a signal composed of multiple frequency-bands, each having a different center-frequency and propagating at a different group velocity [10]–[12]. In this construction, each frequency-band is delayed such that all bands coalesce at the spatial target to produce maximal constructive interference.

This article examines the potential to spatio-temporally focus energy along the waveguide using such a linear combination of pulses propagating at different group velocities. The presented technique demonstrates that the velocity relation governed by (3) can be exploited to generate such a focus at any location along the waveguide. Further, scalability and requirements for optimal configuration are examined and performance predictors are derived in terms of given design parameters. It is shown that this construction is related to wave-packet propagation [13]–[16], which permits treatment of the spatial decay function using asymptotic saddle-point approximations. A numerical simulation corroborates theoretical results. Finally, propagation in an absorptive medium is considered and the effect is demonstrated both in theory and in simulation.

II. Method

The presented technique constructs a signal that generates an excitation peak at a dynamically-adjustable target along a waveguide. Additionally, the signal amplitude and temporal concentration decays with increasing distance from the target. The signal is developed around physical design parameters that are specified by the intended application and are therefore assumed constant. Three parameters pertain directly to the geometry and composite material of the waveguide:

1) L—the longitudinal extent of the waveguide
2) A—a parameter representing the transverse dimension(s) of the waveguide
3) ν_{M}—the theoretical maximum velocity for waves propagating within the waveguide

A fourth parameter, ω_{C} (the waveguide cutoff frequency), is defined by two of the above physical parameters: $\omega_{\mathrm{C}} = \nu_{\mathrm{M}}/A$.

This article employs the following conventions. Spectral frequencies (rad/s) are $\omega.$, velocities (m/s) are $\nu.$, and times (s) are $t.$. Specific frequencies and velocities are related through (3), with $\omega_{\mathrm{MIN}} \leftrightarrow \nu_{\mathrm{MIN}}$ and $\omega_{\mathrm{MAX}} \leftrightarrow \nu_{\mathrm{MAX}}$ respectively representing the minimum and maximum allowed values (by application), and with $\omega_{\mathrm{L}} \leftrightarrow \nu_{\mathrm{L}}$ and $\omega_{\mathrm{H}} \leftrightarrow \nu_{\mathrm{H}}$, respectively, representing the effective lowest and highest values. t_{P} is an optimization parameter representing pulsewidth that is used during signal construction. (Table I lists values for a sample numerical simulation.)

TABLE I
Values of Simulation Parameters

Category	Parameter Name	Value
envelope	$\psi(t)$	$\cos^2(\pi t)\cdot 1_{\{\lvert t\rvert\leq 1/2\}}$
	α	0.01
	W_ω	41.15 rad/s
frequency [rad/s]	ω_{W}	149.01×10^9
	ω_{C}	179.87×10^9
	ω_{MIN}	180.61×10^9
	ω_{L}	255.11×10^9
	ω_{H}	1.72×10^{12}
	ω_{MAX}	1.8×10^{12}
velocity [m/s]	ν_{MIN}	27.26×10^6
	ν_{L}	212.75×10^6
	ν_{H}	298.36×10^6
	ν_{MAX}	298.5×10^6
	ν_{M}	300×10^6
spatial [m]	A	1.67×10^{-3}
	L	1
	z_{T}	0.2, 0.4, 0.6, 0.8 (separate runs)
timing [s]	t_{P}	276.14×10^{-12}
	t_{T}	22.01×10^{-9}
	t_{FOC}	33.33×10^{-9}
	t_{SIM}	36.96×10^{-9}
FFT and sampling	f_{s}	3.55×10^{12} samps/s
	N_{t}	131072
	N_ω	131072
	λ_{min}	1.01×10^{-3} m
	$k_{z_{\mathrm{s}}}$	7.95×10^3 samps/m
	N_{z}	7952

A. Signal Construction

The presented construction exploits the frequency-dependent velocity dispersion of (3) to produce a signal that spatially decays from a target location within the waveguide. This signal is a distribution of amplitude-modulated pulse envelopes propagating at differing group velocities (derived from their respective modulation frequencies). All pulse envelopes are individually delayed such that they produce maximum constructive interference at a predetermined spatial location along the waveguide. Fig. 1 illustrates multiple amplitude-modulated pulses coalescing to produce such a peak. Alternately, each pulse envelope can be considered as a wave packet with static frequency equal to the modulation frequency, traveling along a space-time ray with its respective group velocity. In this framework, the origin of the rays is the spatio-temporal focus. This is developed in Section II.A.3.

1) Pulse Envelope and Characteristics: The presented waveguide signal is constructed as a temporal distribution of pulses, each windowed by the same envelope function. Envelopes considered in this paper are real-valued and nonnegative, have compact support on $t\in[-1/2,1/2]$, and decay symmetrically from a normalized maximum of unity at $t=0$. Let $\psi(t)$ be such an envelope function.

The above restrictions have necessary implications for the approximate spectral width of the pulse. The real-valued, symmetric frequency-band of $\psi(t)$ is given by the Fourier spectrum

$$\Psi(\omega)=\mathcal{F}\{\psi(t)\}=\int_{-\infty}^{+\infty}\psi(t)e^{-\jmath\omega t}dt. \tag{4}$$

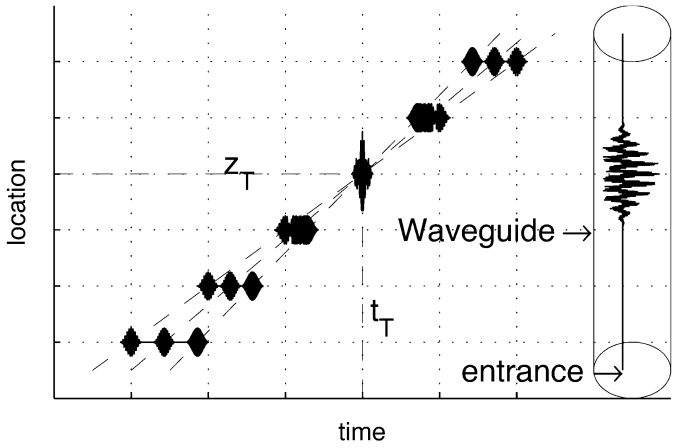

Fig. 1. Illustration of the signal construction scheme for three pulses propagating along a waveguide. The horizontal axis represents time t, increasing from left to right, and the vertical axis represents longitudinal location along the waveguide z, increasing from the waveguide entrance at the bottom to the exit at the top (a reference cylindrical waveguide is depicted along the right of the illustration). The excitation signal, composed of three pulses, enters the waveguide at the lower-left side of the illustration. The three pulses, from left to right, have a respectively low, medium, or high propagation velocity, attained by amplitude modulation with the velocity-respective frequencies given by (3). Dashed lines represent the spatio-temporal path of the center of each pulse as it propagates along the waveguide. The pulses are appropriately delayed such that the pulse centers converge in time at a target location, $z_{\mathrm{T}} = 0.6 \cdot L$. Maximum absolute field intensity over the temporal extent of the signal, as a function of spatial location, is depicted along the reference waveguide.

Because $\psi(t)$ has compact support, $\Psi(\omega)$ cannot have compact support [17]. However, the spectral envelope must decay to zero as $|\omega| \to \infty$ since the total spectral content is bounded ($\int_\omega |\Psi(\omega)|^2 d\omega = 2\pi \int_t |\psi(t)|^2 dt \leq 2\pi$). Let

$$W_\omega = 2 \cdot \omega_\alpha \tag{5}$$

be the approximate width of this spectrum, where ω_α is the smallest positive frequency value such that $|\Psi(\omega)| \leq \alpha \max\{|\Psi|\}\ \forall \omega \geq \omega_\alpha$ (the value is doubled to account for both sides of the symmetric spectrum).[1] Given the above envelope, $\psi(t/t_{\mathrm{P}})$ is a time-scaled envelope with a duration of t_{P}. The nonnegligible spectral width of this scaled envelope is $\omega_{\mathrm{W}}(t_{\mathrm{P}}) = W_\omega / t_{\mathrm{P}}$ because, according to the time and frequency scaling property of the Fourier transform, $\psi(t/t_{\mathrm{P}}) \Leftrightarrow t_{\mathrm{P}} \Psi(\omega t_{\mathrm{P}})$.

2) Pulse Distribution Function: The waveguide signal at a given spatial location is constructed with a uniform distribution of pulse centers. The temporal range of this distribution is implied by (3), which associates low and high group velocity limits (ν_{L} and ν_{H}, respectively) with low and high frequency bounds (ω_{L} and ω_{H}, respectively)

$$\nu_{\{\mathrm{L,H}\}} = \nu_{\mathrm{M}} \sqrt{1 - \left(\omega_{\mathrm{C}} / \omega_{\{\mathrm{L,H}\}}\right)^2}. \tag{6}$$

If, by the construction illustrated in Fig. 1, the centers of the pulse envelopes coalesce at the spatial target z_{T} at time t_{T}, then any pulse-center with associated fixed group velocity $\nu_{\mathrm{L}} \leq \nu_{\mathrm{g}} \leq \nu_{\mathrm{H}}$ will reach any spatial point, z, at time

$$t_{\mathrm{g}}(z, \nu_{\mathrm{g}}) = t_{\mathrm{T}} - \frac{(z_{\mathrm{T}} - z)}{\nu_{\mathrm{g}}}. \tag{7}$$

In particular, this is true for velocity extremes ν_{L} and ν_{H} and defines the temporal range for a given spatial location z: the range is centered at $t_{\mathrm{C}}(z) = (t_{\mathrm{g}}(z, \nu_{\mathrm{H}}) + t_{\mathrm{g}}(z, \nu_{\mathrm{L}}))/2$ and $\Delta t(z) = |t_{\mathrm{g}}(z, \nu_{\mathrm{H}}) - t_{\mathrm{g}}(z, \nu_{\mathrm{L}})|$ is the temporal spread.

The waveguide signal envelope is constructed as a linear combination of pulse envelopes distributed over the above temporal range. Consider N discrete envelopes, evenly spaced across the temporal range producing the signal envelope

$$s_{\psi;N}(t, t_{\mathrm{P}}, z) = \frac{1}{N} \sum_{n=1}^{N} \psi\left(\frac{t - t_{\mathrm{C}}(z) - \Delta t(z)\,[(n-1)/(N-1) - 1/2]}{t_{\mathrm{P}}} \right). \tag{8}$$

This can be interpreted as the output of the convolution

$$s_{\psi;N}(t, t_{\mathrm{P}}, z) = \psi\left(\frac{t}{t_{\mathrm{P}}}\right) * \frac{1}{\Delta t(z)} \phi_N\left(\frac{t - t_{\mathrm{C}}(z)}{\Delta t(z)}\right) \tag{9}$$

$$\phi_N(t) = \frac{1}{N} \sum_{n=1}^{N} \delta\left(t - \left[\frac{n-1}{N-1} - \frac{1}{2}\right]\right) \tag{10}$$

where $\delta(t)$ is the Dirac impulse function. $\phi_N(t)$ is a discrete distribution that is ideally sampled with N samples from the continuous uniform distribution

$$\phi(t) = 1_{\{|t| \leq 1/2\}}. \tag{11}$$

Extending this relationship, the uniform distribution $\phi(t)$ is the limit as the number of samples $N \to \infty$.

$\phi(t)$ is chosen as the temporal distribution for this article because it is optimal in a general sense. It can be shown that $\phi(t)$ asymptotically minimizes the maximum value of s_ψ with increasing temporal spread $\Delta t(z)$.[2] The signal envelope is therefore

$$s_\psi(t, t_{\mathrm{P}}, z) = \psi\left(\frac{t}{t_{\mathrm{P}}}\right) * \frac{1}{\Delta t(z)} \phi\left(\frac{t - t_{\mathrm{C}}(z)}{\Delta t(z)}\right). \tag{12}$$

The following section develops a waveguide input signal for the temporal distribution specified by (11).

3) Waveguide Excitation Signal: The signal at the target spatial focus is constructed as a linear combination of amplitude-modulated pulse envelopes. Amplitude-modulation is required to give each frequency band (associated with a particular pulse envelope) a differing center frequency, which in turn produces differing group velocities by (3). Ultimately, differing group velocities allow a given temporal distribution, and specifically the distribution in (11), to be realized.

[1] Note that W_ω is not equivalent to the normally accepted spectral bandwidth, which might be defined similarly with $\alpha = 1/2$. Here, α should be interpreted as control of precision in the Fourier spectral representation of $\psi(t)$: spectral content that decays past $(1 - \alpha) \times 100\%$ of maximum spectral amplitude is truncated.

[2] For any distribution $f(t) \neq \phi(t)$ with compact support on $t \in [-1/2, 1/2]$, it can be shown that $\exists t_0$ such that $\forall \Delta t > t_0$, $\max_t\{\phi(t/\Delta t) * \psi(t/t_{\mathrm{P}})\} < \max_t\{f(t/\Delta t) * \psi(t/t_{\mathrm{P}})\}$. This is not necessarily optimal for a specific application because it requires a sufficiently large distance from the spatial target. The temporal spread will be constrained if the longitudinal extent of the waveguide is finite, and a nonuniform distribution can yield greater decay over this constrained range. For example, $\phi_N(t)$ in (10) yields smaller maximum intensities up to a certain t_0, and N can be chosen for the application.

The temporal distribution of (11) is mapped to a modulation frequency distribution by successive applications of the chain rule for differentiation. $\phi(t)$ in (11) is a primitive distribution independent of z. Let

$$\phi_t(t_{\rm g}, z) = \frac{\phi\left(\frac{t_{\rm g} - t_{\rm C}(z)}{\Delta t(z)}\right)}{\Delta t(z)} \tag{13}$$

define the shifted and dilated form used to construct $s_\psi(t, z)$ in (12). Define a percentile function $\Phi_t(t_{\rm g}, z)$ such that $\phi_t(t_{\rm g}, z) = d\Phi_t/dt_{\rm g}$. The derivative of (7) with respect to $\nu_{\rm g}$ defines $dt_{\rm g}/d\nu_{\rm g}$ and the derivative of (3) with respect to $\omega_{\rm g}$ defines $d\nu_{\rm g}/d\omega_{\rm g}$. Applying the chain rule and substituting (3) for $\nu_{\rm g}$ yields the modulation frequency distribution

$$\begin{aligned} f^{\rm opt}(\omega_{\rm g}) = \phi_\omega(\omega_{\rm g}) &= \frac{d\Phi_t}{dt_{\rm g}} \cdot \frac{dt_{\rm g}}{d\nu_{\rm g}} \cdot \frac{d\nu_{\rm g}}{d\omega_{\rm g}} \\ &= \frac{\nu_{\rm H}\,\nu_{\rm L}}{\nu_{\rm M}\,\omega_{\rm C}(\nu_{\rm H} - \nu_{\rm L})} \left(\left(\frac{\omega_{\rm g}}{\omega_{\rm C}}\right)^2 - 1\right)^{-3/2} \\ &\quad \cdot 1_{\{\omega_{\rm g} \in [\omega_{\rm L}, \omega_{\rm H}]\}}. \end{aligned} \tag{14}$$

Note that, while $\phi_t(t_{\rm g}, z)$ depends upon spatial location, the dependence cancels out of the relation in (14).

The spectrum of the signal at the spatial focus is constructed using the modulation frequency distribution given by (14). The spectrum of a cosine-modulated pulse envelope is $t_{\rm P}/2\,[\Psi((\omega - \omega_{\rm g})t_{\rm P}) + \Psi((\omega + \omega_{\rm g})t_{\rm P})]$, so it follows that the spectrum of a continuous distribution of modulated pulse envelopes, weighted with density function $\phi_\omega(\omega_{\rm g})$, is

$$\begin{aligned} &S(\omega, t_{\rm P}) \\ &= \frac{t_{\rm P}}{2} \int_{\omega_{\rm g}=-\infty}^{+\infty} [\phi_\omega(\omega_{\rm g}) + \phi_\omega(-\omega_{\rm g})]\Psi((\omega - \omega_{\rm g})t_{\rm P}) d\omega_{\rm g}. \end{aligned} \tag{15}$$

Note that S is real-valued and symmetric because it is the convolution of two real-valued, symmetric functions. Therefore, the individual components of S are not relatively phase-delayed but are all centered at $t = 0$. Since this formulation of pulse envelopes with differing modulation frequencies and, therefore, differing group velocities contains no temporal spread, $S(\omega, t_{\rm P})$ is the signal at the spatial focus $z_{\rm T}$. This fact confirms the earlier assertion that the origin of the space-time rays is the spatio-temporal focus. Under this viewpoint, the rays must extend backward in time to induce the waveguide excitation signal.

The spectrum of the waveguide excitation signal is

$$I(\omega, t_{\rm P}) = S(\omega, t_{\rm P}) e^{\jmath \beta'(\omega) z_{\rm T}}\, e^{-\jmath\omega\,(t_{\rm T} + t_{\rm P}/2)}. \tag{16}$$

Here, $t_{\rm T} = z_{\rm T}/\nu_{\rm MIN}$ is the amount of time it will take the minimum frequency energy to propagate from the waveguide entrance to the target $z_{\rm T}$, and

$$\beta'(\omega) = \begin{cases} \beta(\omega) & \omega_{\rm MIN} \le |\omega| \le \omega_{\rm MAX} \\ 0 & \text{otherwise} \end{cases} \tag{17}$$

is a modified propagation constant that only adjusts elements within some allowed frequency range $\omega \in [\omega_{\rm MIN}, \omega_{\rm MAX}] \cdot$ $\omega_{\rm MIN}$ and $\omega_{\rm MAX}$ respectively denote the application specific minimum[3] and maximum allowed frequencies, with associated group velocities $\nu_{\rm MIN}$ and $\nu_{\rm MAX}$. The first exponential term in (16) compensates for group dispersion by inverting the waveguide transfer function (backprojecting the space-time rays), while the second exponential term sets the beginning of the signal at $\{t = 0,\, z = 0\}$.

The input signal is given by the inverse Fourier transform

$$\begin{aligned} i(t, t_{\rm P}) &= \mathcal{F}^{-1}\{I(\omega, t_{\rm P})\} \\ &= \frac{1}{2\pi} \int_{-\infty}^{+\infty} I(\omega, t_{\rm P}) e^{\jmath\omega t} d\omega. \end{aligned} \tag{18}$$

Note that $z_{\rm T}$ is a parameter in the construction of the input signal spectrum given in (16). This indicates that once the spectrum S is established for a given application, the spatial target can be adjusted dynamically with the linear filtering step in (16).

B. Optimal Signal Parameters

It is desirable to derive the signal parameters that minimize the maximum signal intensity away from the spatial target, $z_{\rm T}$. Section II-A–3 demonstrates that a waveguide input signal exists that produces at the spatio-temporal target the temporal distribution $\phi(t)$ in (11). The free parameters for this construction are $t_{\rm P}, \omega_{\rm L}, \omega_{\rm H}, \omega_{\rm MAX}$, and $\omega_{\rm MIN}$, with $\omega_{\rm C} \le \omega_{\rm MIN} \le \omega_{\rm L} \le \omega_{\rm H} \le \omega_{\rm MAX}$, which were assumed in Section II-A–3.

The maximum signal intensity can be approximated by upper-bounds in two regions. The first region is near the target, where the primary decay in signal intensity is the result of inter-pulse spreading. Neglecting phase interference, the maximum value of the signal envelope in (12) occurs at $t = t_{\rm C}(z)$ and is

$$\sigma_1(t_{\rm P}, z) = \frac{1}{\Delta t(z)} \int_{-\Delta t(z)/2}^{\Delta t(z)/2} \psi\left(\frac{t}{t_{\rm P}}\right) dt. \tag{19}$$

$\sigma_1(t_{\rm P}, z)$ represents the spatial decay of the signal envelope propagating along the waveguide. Let

$$\mathcal{C}(t_{\rm P}, z) = \frac{\Delta t(z)}{t_{\rm P}} = \frac{|z - z_{\rm T}|}{t_{\rm P}} \left(\frac{1}{\nu_{\rm L}} - \frac{1}{\nu_{\rm H}}\right) \tag{20}$$

define temporal capacity of the pulse spread, i.e., the number of distinct pulse envelopes of duration $t_{\rm P}$ that can fit without overlap into the temporal spread at z. As will be shown, parameter optimization reduces to maximizing $\mathcal{C}$. Setting $k = t/t_{\rm P}$, (19) is rewritten in terms of $\mathcal{C}$

$$\sigma_1(t_{\rm P}, z) = \frac{1}{\mathcal{C}(t_{\rm P}, z)} \int_{-\mathcal{C}(t_{\rm P}, z)/2}^{\mathcal{C}(t_{\rm P}, z)/2} \psi(k) dk. \tag{21}$$

The second upper-bound is located in a region sufficiently displaced from the target such that intrapulse dispersion becomes significant. In this region, the distance is sufficient to permit so-called "saddle-point" approximations of the traveling wave packets corresponding to the lower frequency bands [13]–[15]. Following this method, each wave packet undergoes dispersion while traveling a space-time ray at its corresponding

[3]Frequencies below $\omega_{\rm MIN}$ will propagate too slowly or will be attenuated because they are below cutoff. See Section II-B for more details.

group velocity.[4] The saddle-point contribution to the field of the time-harmonic wave packet is[5]

$$P(\omega_g, t_P, z) = 2\Re\left\{ S(\omega_g, t_P) \times \left[-\jmath 2\pi z \left. \frac{d^2}{d\omega^2}\beta(\omega)\right|_{\omega=\omega_g} \right]^{-1/2} e^{-\jmath z\beta(\omega_g)} \right\} \quad (22)$$

noting that $S(\omega_g, t_P) = t_P/2[\phi_\omega(\omega) + \phi_\omega(-\omega)] * \Psi(\omega t_P)|_{\omega=\omega_g}$. The total signal field is then approximately

$$i(t, t_P, z) \approx \frac{1}{2\pi}\int_{-\infty}^{\infty} P(\omega, t_P, z) e^{\jmath\omega t} d\omega. \quad (23)$$

To determine an upper bound, apply the identity $|\int f(x)dx| \leq \int |f(x)|dx$ to (23), yielding

$$\sigma_2(t_P, z) = \frac{1}{\pi\mathcal{C}(t_\mathrm{P}, z)}\sqrt{\frac{\omega_C|z - z_T|}{\pi\nu_\mathrm{M}}} \times \int_{-\infty}^{\infty}\left[\left(\frac{\omega}{\omega_C}\right)^2 - 1\right]^{3/4} \times \{[\phi_\omega(\omega) + \phi_\omega(-\omega)] * \Psi(\omega t_P)\} d\omega \quad (24)$$

as with σ_1, this approximate bound neglects local phase interference.[6]

Parameter optimization is achieved by maximizing temporal capacity. In both regions, the spatial decay is inversely proportional to $\mathcal{C}$. In the case of σ_1, this relation is scaled by integration over a central region of the pulse envelope, ψ. But, in the case of decaying envelopes, the rate of contribution from the integral diminishes as the region of integration increases; so increasing $\mathcal{C}$ decreases the total bound. In the case of σ_2, the spectral width of the pulse is expected to be small compared with the overall distribution ϕ_ω. Hence, the integral may be approximated as constant, and this bound also decreases with increasing $\mathcal{C}$. Therefore, the optimization goal to minimize field intensity away from z_T is accomplished by maximizing $\mathcal{C} \forall\, z \neq z_\mathrm{T}$, independent of $\psi(t)$.

For fixed t_P, maximizing $\mathcal{C}$ is reduced to maximizing the temporal spread, Δt. Since the possible velocities are bounded $(0 < \nu_\mathrm{MIN} < \nu_\mathrm{L} < \nu_\mathrm{H} < \nu_\mathrm{MAX} < \nu_\mathrm{M})$, maximizing velocity spread, $\nu_\mathrm{H} - \nu_\mathrm{L}$, achieves maximum temporal spread, and velocity spread is maximized by maximizing the frequency spread, $\omega_\mathrm{H} - \omega_\mathrm{L}$. Hence, the low and high pulse center-frequencies are respectively set as low and as high as possible; i.e., $\omega_\mathrm{L} = \omega_\mathrm{MIN} + \omega_\mathrm{W}(t_\mathrm{P})/2$ and $\omega_\mathrm{H} = \omega_\mathrm{MAX} - \omega_\mathrm{W}(t_\mathrm{P})/2$.

However, because of the functional dependence of spectral width upon pulse duration (i.e., $\omega_\mathrm{W}(t_\mathrm{P}) = W_\omega/t_\mathrm{P}$), the minimum and maximum group velocities also vary with pulse duration. For a given bandwidth

$$\omega_\mathrm{L}(t_\mathrm{P}) = \omega_\mathrm{MIN} + \frac{W_\omega}{2t_\mathrm{P}} \quad (25)$$

and

$$\omega_\mathrm{H}(t_\mathrm{P}) = \omega_\mathrm{MAX} - \frac{W_\omega}{2t_\mathrm{P}}. \quad (26)$$

Equation (6) extends this dependence from $\omega_{\{\mathrm{L,H}\}}$ to the group velocities $\nu_{\{\mathrm{L,H}\}}$. Incorporating (6), (25), and (26) into (20) yields

$$\mathcal{C}(t_\mathrm{P}, z) = \frac{|z - z_\mathrm{T}|}{\nu_\mathrm{M}\, t_\mathrm{P}}\left[\left(1 - \left(\frac{\omega_\mathrm{C}}{\omega_\mathrm{MIN} + W_\omega/2t_\mathrm{P}}\right)^2\right)^{-1/2} - \left(1 - \left(\frac{\omega_\mathrm{C}}{\omega_\mathrm{MAX} - W_\omega/2t_\mathrm{P}}\right)^2\right)^{-1/2}\right]. \quad (27)$$

An analytic solution for the optimal pulse duration, $t_\mathrm{P}^\mathrm{opt}$, is obtained by allowing ω_MIN and ω_MAX to achieve their respective limits. The center frequency distribution given in (14) exhibits a cubic decay to zero with increasing ω. Hence, for $(\omega/\omega_\mathrm{C})^2 \gg 1$, $\phi_\omega(\omega)/\phi_\omega(\omega_\mathrm{L}) \approx 0$. As $\omega_\mathrm{MAX} \to \infty$, $\nu_\mathrm{MAX} \to \nu_\mathrm{M}$, reducing the second term in (27) to unity. In contrast, ω_MIN cannot be lower than ω_C, and if $\omega_\mathrm{MIN} = \omega_\mathrm{C}$, the lowest propagation velocity is $\nu_\mathrm{MIN} = 0$. However, if $\alpha \approx 0$ in (5), the majority of the signal will have a nonzero propagation velocity ($\omega_\mathrm{L} = \omega_\mathrm{MIN} + W_\omega/2t_\mathrm{P}$). These two reductions yield the greatest possible velocity spread while also simplifying the temporal capacity equation such that

$$\mathcal{C}(t_\mathrm{P}, z) \approx \frac{|z_\mathrm{T} - z|}{\nu_\mathrm{M}\, t_\mathrm{P}}\left[\left(1 - \left(1 + \frac{W_\omega}{2\omega_\mathrm{C} t_\mathrm{P}}\right)^{-2}\right)^{-1/2} - 1\right]. \quad (28)$$

The maxima of (28) are located at peaks such that $d\mathcal{C}/dt_\mathrm{P} = 0$, and only one $t_\mathrm{P} > 0$ satisfies this relationship $\forall z$

$$t_\mathrm{P}^\mathrm{opt} = \frac{W_\omega}{2\omega_\mathrm{C}(\sqrt{2} - 1)}. \quad (29)$$

Substituting $t_\mathrm{P}^\mathrm{opt}$ back into (28) yields

$$\mathcal{C}^\mathrm{opt}(z) = \max_{t_\mathrm{P}>0}\mathcal{C}(t_\mathrm{P}, z) = \frac{2|z - z_\mathrm{T}|}{A\, W_\omega(3 + 2\sqrt{2})}. \quad (30)$$

The choice of frequency range is related to the overall focusing time of successive input signals (e.g., in the case of multiple spatial targets). The frequency range bounds are ω_MIN and ω_MAX, which in reality correspond respectively to velocities $\nu_\mathrm{MIN} > 0$ and $\nu_\mathrm{MAX} < \nu_\mathrm{M}$. Wave energies at these lowest and highest frequencies respectively require L/ν_MIN and L/ν_MAX time to reach the end of the waveguide. Let the focus time t_FOC be the delay between successive signals such that the fastest wave energy of the second signal reaches the slowest energy of the first signal at the end of the guide, thus, avoiding interaction

$$t_\mathrm{FOC} = \frac{L}{\nu_\mathrm{MIN}} - \frac{L}{\nu_\mathrm{MAX}}. \quad (31)$$

[4]Because the medium is ideally nonabsorptive, the group velocity is uniquely specified. In the case of an absorptive medium, group velocity is not uniquely defined [18].

[5]This is a reduced form of [13, eq. (1.84)].

[6]Note that the upper bound in (24) is proportional to $\sqrt{|z - z_T|}/\mathcal{C}(t_P, z)$, with $\mathcal{C}(t_P, z)$ proportional to z. Hence, the upper bound is actually proportional to $1/\sqrt{|z - z_T|}$, as expected for expanding wave packets.

If t_{FOC} is specified by the application, it defines the minimum velocity and also the minimum frequency since

$$\nu_{\mathrm{MIN}} = \frac{L}{t_{\mathrm{FOC}} + L/\nu_{\mathrm{MAX}}} = \nu_{\mathrm{M}}\sqrt{1 - \left(\frac{\omega_{\mathrm{C}}}{\omega_{\mathrm{MIN}}}\right)^2}. \quad (32)$$

The optimal results given in (29) and (30) were obtained by assuming that the focus time and the maximum allowable frequency were both sufficiently large. Stating that $t_{\mathrm{FOC}} \gg L/\nu_{\mathrm{MAX}}$ is identical to stating that the lowest velocity is much lower than the maximum velocity: $\nu_{\mathrm{MIN}} \ll \nu_{\mathrm{MAX}}$. This is a consistent restatement of the original goal of maximum temporal spread. Similarly, $\omega_{\mathrm{MAX}} \gg \omega_{\mathrm{W}}$ is identical to $\omega_{\mathrm{H}} \gg \omega_{\mathrm{L}}$ since $\omega_{\mathrm{L}} \approx \omega_{\mathrm{C}} + \omega_{\mathrm{W}}/2$; this is again the goal of maximum temporal spread since $\omega_{\mathrm{H}} \gg \omega_{\mathrm{L}} \rightarrow \nu_{\mathrm{H}} \gg \nu_{\mathrm{L}}$ when $\omega_{\mathrm{L}} \approx \omega_{\mathrm{C}}$. However, there is a decreasing benefit to increasing either t_{FOC} or ω_{MAX}, since ω_{L} becomes bandwidth dominated when $\omega_{\mathrm{MIN}} \approx \omega_{\mathrm{C}}$, while $\lim_{\omega_{\mathrm{MAX}}\rightarrow\infty} \nu_{\mathrm{MAX}} = \nu_{\mathrm{M}}$ and $\phi_\omega(\omega)/\phi_\omega(\omega_{\mathrm{L}}) \approx 0, \forall (\omega/\omega_{\mathrm{C}})^2 \gg 1$. Hence, choosing t_{FOC} and ω_{MAX} one or two orders of magnitude above L/ν_{M} and ω_{C}, respectively, will ensure nearly optimal results without requiring infinite bandwidth or duration.

Finally, the optimal specification for pulse duration ensures that the spectral width of the pulse-envelope, and the lower bounds to frequency and velocity, are all independent of the choice of envelope. Noting that $\omega_{\mathrm{W}} = W_\omega/t_{\mathrm{P}}$ yields

$$\omega_{\mathrm{W}}^{\mathrm{opt}} = 2\omega_{\mathrm{C}}(\sqrt{2} - 1). \quad (33)$$

If t_{FOC} is sufficiently large such that $\omega_{\mathrm{MIN}} \approx \omega_{\mathrm{C}}$, then

$$\omega_{\mathrm{L}}^{\mathrm{opt}} \approx \omega_{\mathrm{C}}\sqrt{2} \quad (34)$$

which leads to the velocity bound

$$\nu_{\mathrm{L}}^{\mathrm{opt}} \approx \frac{\nu_{\mathrm{M}}}{\sqrt{2}}. \quad (35)$$

C. Signal Attenuation due to Absorption

Since the presented signal construction assumes a lossless propagation medium, it is important to consider the effect of an absorptive medium upon performance. This effect is considered in terms of the intended peak intensity at the spatio-temporal focus. If the signal accrues attenuation during propagation, it is desirable that this attenuation be small compared with the intended signal gain at the focus.

An absorptive medium can be modeled with complex permittivity, resulting in a complex scale factor in the propagation relation. In a lossless medium, $\nu_M = (\mu\epsilon)^{-1/2}$, and the effect of losses can be incorporated into the permittivity, ϵ, such that $\epsilon = \epsilon' - \jmath\epsilon''$, with $\epsilon', \epsilon'' > 0$. Let $\rho = \epsilon''/\epsilon'$ be a resistivity coefficient, then $\nu_M^{(l)} \leftarrow \nu_M/\sqrt{1-\jmath\rho}$ and $\omega_C^{(l)} \leftarrow \omega_C/\sqrt{1-\jmath\rho}$ are updated parameters that reflect the affect of the absorptive medium. It follows that the propagation relation is updated to

$$\beta^{(l)}(\omega) = \frac{1}{A}\sqrt{(1-\jmath\rho)\left(\frac{\omega}{\omega_C}\right)^2 - 1} \quad (36)$$

where $\omega_C = \nu_M/A$.[7] Here ρ induces an imaginary part in $\beta^{(l)}$ that contributes frequency-dependent attenuation to the propagating signal. The first two terms of a binomial expansion for $\beta^{(l)}$ approximate the real (propagating) and imaginary (attenuating) components:

$$\beta^{(l)}(\omega) \approx \frac{1}{A}\left(\left(\frac{\omega}{\omega_C}\right)^2 - 1\right)^{1/2} - \jmath\frac{\rho\omega^2}{2A}\left(\left(\frac{\omega}{\omega_C}\right)^2 - 1\right)^{-1/2}. \quad (37)$$

The presented signal construction remains robust if propagation losses are sufficiently below the expected gain, i.e., if $\rho < \rho_E$. ρ_E signifies the resistivity at which propagation losses at the spatial target are equal to the expected system gain. Signal attenuation is approximated using the imaginary component in (37) and then compared with the upper bound $\sigma_2(z)$ in (24) to estimate ρ_E. In the signal construction, the majority of the signal energy is located near $\omega = \omega_L$, with $\omega_{\mathrm{L}}^{\mathrm{opt}} \approx \omega_{\mathrm{C}}\sqrt{2}$ in (34). While the imaginary part of (37) grows linearly with ω, the relative amplitude of the signal is inversely proportional to ω^3 in (14). Hence, the overall signal attenuation can be represented with the attenuation for $\omega = \omega_L^{\mathrm{opt}}$. At this frequency, the signal is attenuated by the factor $\exp(-\rho z/A)$. ρ_E is estimated by the relation

$$e^{-\rho_E z_T/A} = \sigma_2(0) \quad (38)$$

noting that $\sigma_2(0)$ is the upper bound of the signal strength at the waveguide entrance, relative to a maximum of unity at the spatial target z_T. Hence

$$\rho_E = -\frac{A}{z_T}\log\sigma_2(0). \quad (39)$$

The affect of absorption will become noticeable as $\rho \rightarrow \rho_E$.

III. Simulation and Numeric Results

To illustrate the above analytic results, signals constructed according to (18) were numerically simulated propagating along a waveguide. While the above analysis defines $t_{\mathrm{P}}^{\mathrm{opt}}$ and ϕ_ω, and gives recommendations for t_{FOC} and ω_{MAX}, several simulation parameters were specifically chosen for these simulations. These choices are intended to 1. demonstrate the interaction of various parameters in the signal construction and 2. provide numerical corroboration of the theoretical analysis. The waveguide length was chosen $L = 1$m, and the theoretical maximum propagation velocity was $\nu_{\mathrm{M}} = 300 \times 10^6$ m/s (free space). Four separate simulations were run with spatial targets of $z_{\mathrm{T}} = 0.2, 0.4, 0.6$, and 0.8 m, respectively.

The Hanning window [19]

$$\psi(t) = \cos^2(\pi t)\cdot 1_{\{|t|\leq 1/2\}} \quad (40)$$

[7]This is consistent with more exact analysis of absorptive losses (e.g., in [14] and [15]). However, analysis here diverges from such methods to obtain a simple approximation of the performance of the ideal signal construction in absorptive media.

was chosen as the simulation envelope. The Fourier spectrum of this envelope is

$$\Psi(\omega) = \frac{\sin(\omega/2)}{\omega[1-(\omega/2\pi)^2]}, \tag{41}$$

which has a maximum value of 1/2 at $\omega = 0$ and an accurate absolute bound of $|\omega^{-1}[1-(\omega/2\pi)^2]^{-1}|$ for $|\omega| > 2\pi$. $\alpha = 0.01$ was set for (5) and W_ω was approximated with twice the real root to the cubic equation $-2/\alpha = \omega[1-(\omega/2\pi)^2]$: $W_\omega \approx 41.15$ rad/s.[8]

With the Hanning envelope, the spatial decay bounds given by (21) and (24) become

$$\sigma_1(z) = \frac{1}{2}\begin{cases} 1+\sin(\pi\mathcal{C}^{\rm opt}(z))/\pi\mathcal{C}^{\rm opt}(z), & \mathcal{C}^{\rm opt}(z) \le 1 \\ 1/\mathcal{C}^{\rm opt}(z), & \mathcal{C}^{\rm opt}(z) > 1 \end{cases} \tag{42}$$

and

$$\sigma_2(z) \approx \frac{K(1/\sqrt{2})}{8\pi\mathcal{C}^{\rm opt}(z)}\sqrt{\frac{\omega_{\rm C}|z-z_T|}{\pi\nu_{\rm M}}}, \tag{43}$$

where $K(1/\sqrt{2})$ is the complete elliptic integral of the first kind with modulus $1/\sqrt{2}$. The approximation of σ_2 results from treating the pulse spectrum as an effective impulse, allowing the signal spectrum S to be approximated with ϕ_ω in (24), with $\omega_L/\omega_C = \sqrt{2}$ and ω_H left unbounded.

The transverse parameter A was chosen to yield a specific spatial resolution, which also defined $\omega_{\rm C}$ and $t_{\rm P}^{\rm opt}$. Using σ_1, the maximum value of the signal envelope decays to 1/2 when $\mathcal{C}^{\rm opt}(z) = 1 \cdot A$ was chosen so that the spatial envelope would be 1/2 at 20% of the waveguide length away from the target. That is, while A might normally be specified by the application, for the purposes of this simulation it was determined so that $\mathcal{C}^{\rm opt}(z_{\rm T} \pm 20/100 \cdot L) = 1$. Using (30),

$$A = \frac{2 \cdot 20/100 \cdot L}{W_\omega(3+2\sqrt{2})} \approx 1.67 \times 10^{-3}\text{m}. \tag{44}$$

This led to the cutoff frequency $\omega_{\rm C} = \nu_{\rm M}/A = 179.87 \times 10^9$ rad/s and to the optimal pulse duration $t_{\rm P}^{\rm opt} \approx 276.14 \times 10^{-12}$s by (29).

$t_{\rm FOC}$ and $\omega_{\rm MAX}$ were both chosen to be sufficiently large. In (14) when $\omega = 10 \cdot \omega_{\rm C}$, $\phi_\omega(\omega)/\phi_\omega(\omega_{\rm L}) \approx \phi_\omega(10)/\phi_\omega(\sqrt{2}) \approx 99^{-3/2} \approx 0.001 \approx 0$, so $\omega_{\rm MAX} = 10 \cdot \omega_{\rm C} \approx 1.8 \times 10^{12}$ rad/s is sufficiently large. Similarly, $t_{\rm FOC}$ was set to $10 \cdot L/\nu_{\rm M} \approx 33.33 \times 10^{-9}$ s, which is an order of magnitude greater than the time required for a pulse propagating at maximum velocity to reach the end of the waveguide.

Having characterized the waveguide and signal parameters, the rest of the simulation parameters were derived from the above-defined functional relations. Table I lists the completed set of simulation parameters.

The simulation was conducted using the fast-Fourier transform (FFT). The overall simulation time was set to the amount of time required for the energy propagating at velocity $\nu_{\rm MIN}$ to cross the waveguide, plus the pulse duration: $t_{\rm SIM} = L/\nu_{\rm MIN} +$ $t_{\rm P}^{\rm opt}$.[9] Temporal sampling was conducted at a rate at least 4 times the Nyquist frequency (in Hz, $\omega_{\rm MAX}/\pi$), but the actual rate, f_s, was adjusted up so that $N_t = N_\omega$, the number of samples, was a power of 2 to facilitate the FFT. Frequency was sampled on a symmetric range $-\pi f_s \le \omega < \pi f_s$. Spatial sampling was similarly constructed by identifying the smallest wavelength $\lambda_{\rm min} = \min\{\lambda \,|\, \lambda = 2\pi\nu_{\rm M}\sqrt{1/\omega^2 - 1/\omega^4}, \forall\omega \in [\omega_{\rm MIN}, \omega_{\rm MAX}]\}$,[10] and selecting N_z samples at the spatial rate $k_{z_s} = \lceil 4 \cdot 2/\lambda_{\rm min} \rceil$ across $0 \le z \le L(L = 1\text{m})$. All discrete functions were considered ideally sampled.

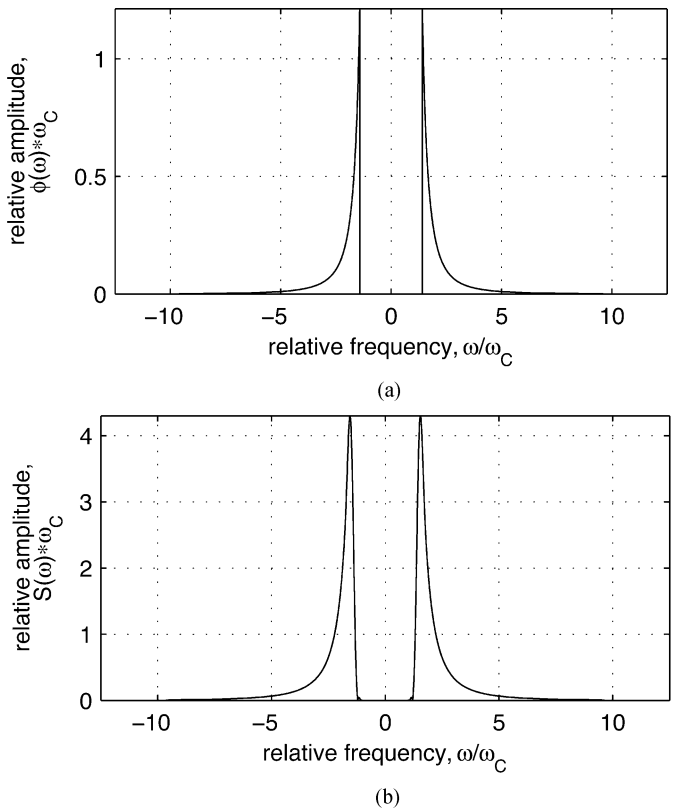

Fig. 2. Plots of the waveguide input signal spectrum construction for the simulation. (a) The symmetric spectral distribution function $\phi(\omega)/2 + \phi(-\omega)/2$. (b) The spectrum of the signal at the spatial focus (result of convolution), $S(\omega)$.

The waveguide signal at the input and other locations was constructed by following Section II-A–3. The pulse envelope spectrum $\Psi(\omega \cdot t_{\rm P}^{\rm opt})$, modulation frequency distribution $\phi_\omega(\omega)$, original and modified propagation relations $\beta(\omega)$ and $\beta'(\omega)$, and waveguide transfer function $H(\omega, z)$ were all computed directly from (41), (14), (1), (17), and (2), respectively, on the sampled ω values. The spectrum of the waveguide excitation signal at the target S was computed as in (15) with discrete convolution using the truncated envelope $\Psi(\omega \cdot t_{\rm P}^{\rm opt})$, $\omega \in [-\omega_{\rm W}, \omega_{\rm W}]$. Fig. 2(a) and (b), respectively, illustrates the distribution $\phi_\omega(\omega)$ and the spectrum $S(\omega)$. The spectra of the waveguide signal at the input and other locations within the waveguide were directly computed using (16) and application

[8]Note that α is required to be small (i.e., $\alpha \approx 0$), by the optimization in Section II.B. Hence, W_ω should not be taken as the bandwidth. Instead, it signifies the nonnegligible region of the signal.

[9]In practice, with $\nu_{\rm L} \approx 10 \cdot \nu_{\rm MIN}$ (see Table I), this is perhaps one order of magnitude in excess of the required simulation interval for significant signal levels.

[10]$\lambda = 2\pi\nu/\omega$. By (3), $\lambda = 2\pi\nu_{\rm M}\sqrt{1-1/\omega^2}\,/\,\omega$.

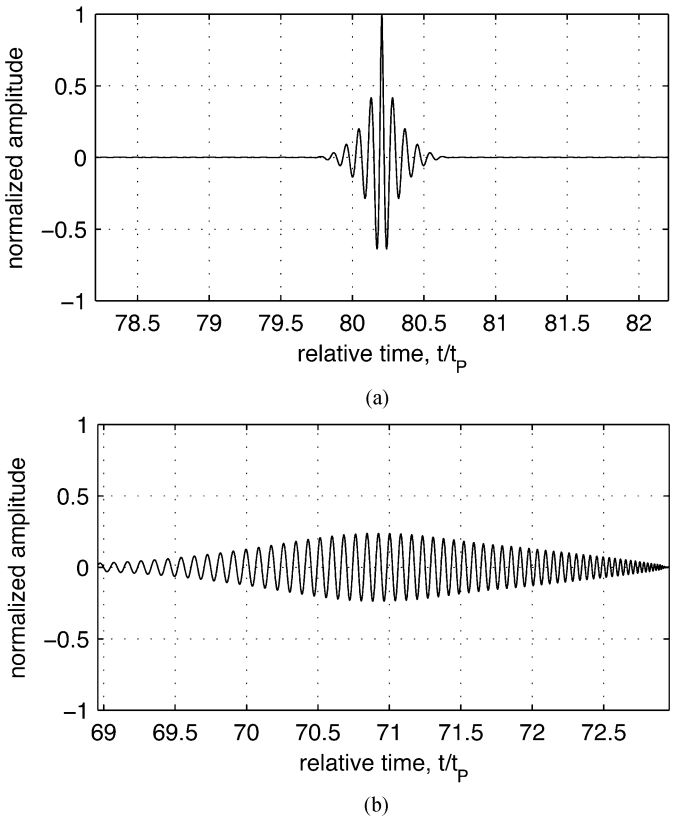

Fig. 3. Plots of the constructed waveguide signal for the simulation. (a) The constructed temporal signal at the spatial focus. (b) The waveguide input signal. (Note that the horizontal axis is time in units relative to pulsewidth, $t/t_{\rm P}$, for (a) and (b), and the scale is the same.)

of the waveguide transfer function $H(\omega, z)$. All temporal signals were approximated from their corresponding spectra using the inverse-FFT (IFFT) function. Fig. 3(a) and (b) illustrate the constructed signal at the spatial focus and at the waveguide entrance, respectively, for $z_{\rm T} = 0.6$m.

Each simulation consisted of sampling the temporal waveguide signal at every spatial sampling point $0 \leq z_n \leq 1$, $n = 1 \ldots N_z$. This sampling was performed by multiplying the spectrum of the input signal with $H(\omega, z_n)$ and then computing the temporal signal via IFFT. Fig. 4 illustrates the simulation results for $z_{\rm T} = 0.6$m, with the spatio-temporal absolute field intensity depicted in Fig. 4(a) and (b), the spatial maximum absolute field intensity depicted in Fig. 4(c), and the temporal maximum absolute field intensity depicted in Fig. 4(d). The combined spatial decay bound from (42) and (43) is also shown in Fig. 4(c).

Simulations were also run with sub-optimal maximum frequency, $\omega_{\rm MAX} = [2, 3, 4, 5] \cdot \omega_{\rm C}$. Together with $\omega_{\rm MAX} = 10 \cdot \omega_{\rm C}$, these represent signal bandwidths of approximately $[1, 2, 3, 4, 9] \cdot \omega_{\rm C}$, respectively. Fig. 5 illustrates the degradation of spatial decay performance with decreasing signal bandwidth for a spatial target of $z_{\rm T} = 0.6{\rm m}$.

Fig. 6 reproduces Fig. 4(c) for each of the target locations, showing the same spatial roll-off but recentered at each of the target locations. Note that the maximum field strength is attained at each of the target locations, and the spatial decay does not change as a function of target location. Results are similar for signal bandwidths of $\sim [1, 2, 3, 4] \cdot \omega_{\rm C}$ (not shown).

Finally, simulations were performed with absorptive media as characterized by the absorptive propagation relation in (36). The resistivity equivalence point ρ_E was estimated using (39) in conjunction with the simulation specific, approximate upper-bound σ_2 in (43); for this simulation, $\rho_E \approx 3.71 \times 10^{-3}$. Using this value, simulations were performed with resitivity coefficients $\rho = [0.1, 0.5, 1] \cdot \rho_E$. Fig. 7 illustrates the results of these simulations. At $\rho = 0.1\,\rho_E$, the spatial response is only slightly attenuated in comparison with $\rho = 0$ (also drawn for reference). This attentuation increases with increasing ρ, as seen in the $\rho = 0.5\,\rho_E$ and $\rho = \rho_E$ curves. ρ_E is a fairly close approximation of the actual resistivity that would provide equivalent attenuation to the expected system gain: in Fig. 7, the peak in the $\rho = \rho_E$ curve is only slightly lower than the maximum intensity of the signal at input (dashed line).

IV. Discussion

A method was presented that exploits the frequency-dependent velocity dispersion inherent to waveguides in order to produce a spatio-temporal focus at any spatial target along the longitudinal extent of the waveguide. The target location can be manipulated by modifying the waveguide input signal through a linear filtering step, where the filter is dependent upon the target location and is related to the waveguide transfer function. This means that the underlying waveguide structure can remain fixed, while still allowing any spatial point to be targeted. Such a system may be useful in a variety of applications that use spatio-temporally focused energy as a catalyst to achieve a desired system activation.

A. Summary of Analysis

Analysis of the presented waveguide signal construction reveals two effects of the choice of the physical waveguide parameters. First, the results scale in proportion to the waveguide cutoff frequency $\omega_{\rm C} = \nu_M/A$. The overall signal bandwidth covers the region from $\omega_{\rm C}\sqrt{2}$ to approximately one order of magnitude above ω_C. The upper bound is due to the modulation frequency distribution in (14), which is inversely proportional to $(\omega/\omega_C)^3$ for $(\omega/\omega_C)^2 \gg 1$. (In simulation, an upper frequency limit of $\omega_H = 3 \cdot \omega_C$ produced qualitatively similar results to $\omega_H = 10 \cdot \omega_C$.) Also, signal times are inversely proportional to ω_C. In particular, the optimal duration of each constituent pulse is $t_P = W_\omega/(2\omega_C(\sqrt{2}-1))$ in (29) and the maximum time for each pulse is $t_{\rm FOC} = L/A \cdot (\sqrt{2}-1)/\omega_C$. Second, while the relationship between maximum field amplitude and distance from the spatial target is complex, the asymptotic spatial decay is influenced by the transverse parameter A. At sufficient distances from the spatial target, the field is bounded by σ_2 in (24). After some rearrangement, this relation reduces to $\sigma_2(z) \propto \sqrt{A/|z_T - z|}$.

Note that σ_2 is only relevant at sufficient distances from the target. At distances arbitrarily close to the target, σ_2 is unbounded and arbitrarily large. In these regions, the upper bound σ_1 in (21) is more precise, and indeed agrees exactly with the simulation at the target [see Fig. 4(c)]. As noted previously, σ_1

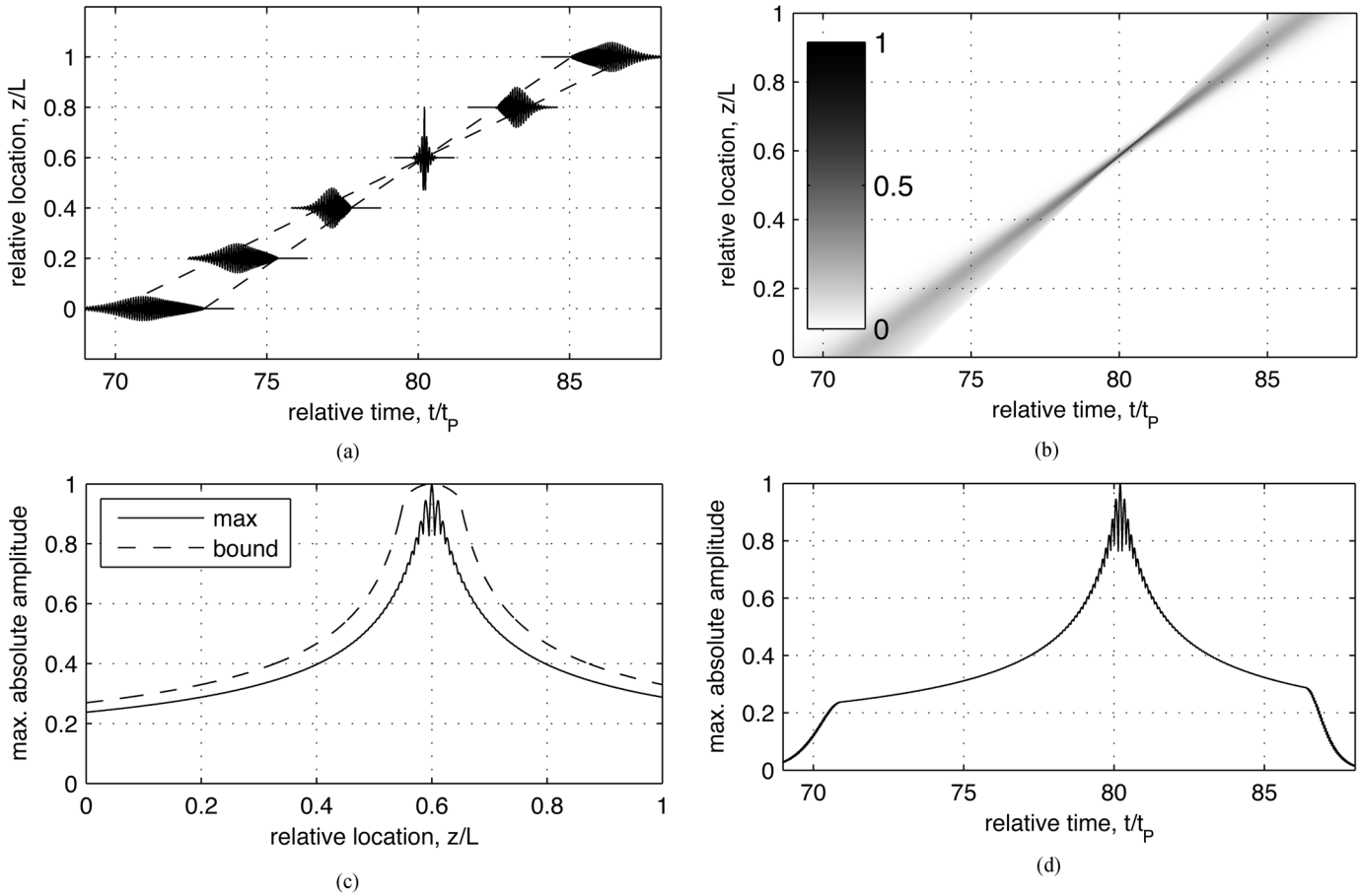

Fig. 4. Results of the spatio-temporal simulation. (a) Spatio-temporal visualization of the waveguide signal as it propagates through the waveguide with spatial target $z_{\mathrm{T}} = 0.6$. The horizontal axis is time in units relative to pulsewidth (t/t_{P}), and the vertical axis is relative longitudinal distance (z/L); this is the same arrangement as in Fig. 1. (Note that only the temporal subset $[t_{\mathrm{T}} - z_{\mathrm{T}}/\nu_{\mathrm{L}} - t_{\mathrm{P}}/2, t_{\mathrm{T}} - (z_{\mathrm{T}} - 1)/\nu_{\mathrm{L}} + t_{\mathrm{P}}/2]/t_{\mathrm{P}}$ is displayed on the horizontal axis.) Dashed lines depict the spatio-temporal paths of the slowest (ν_{L}) and fastest (ν_{H}) pulses. (b) Horizontal and vertical axes are the same as in (a). Absolute field intensity is depicted with gray-shading (see inset colorbar). Horizontal and vertical axes are the same as in 4(a). (c) Maximum absolute field intensity as a function of relative longitudinal distance. The horizontal axis is distance (z/L); the vertical axis is maximum absolute field intensity across the entire time-series. The solid line indicates the simulation results while the dashed line indicates the combined predicted spatial decay of (42) and (43). (d) Maximum absolute field intensity as a function of relative time. The horizontal axis is time (t/t_{P}) in the same range as the horizontal axis of the spatio-temporal plots; the vertical axis is maximum absolute field intensity across the entire space-series.

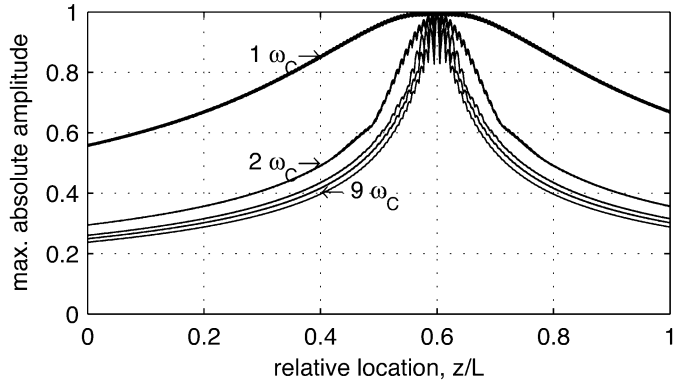

Fig. 5. Spatial results from suboptimal (i.e., lower) signal bandwidth. Data from $\omega_{\mathrm{MAX}} = [2, 3, 4, 5, 10] \cdot \omega_{\mathrm{C}}$ (leading to bandwidths of approximately $[1, 2, 3, 4, 9] \cdot \omega_{\mathrm{C}}$, respectively) are superimposed and displayed the same as in Fig. 4(c). The spatial target was $z_{\mathrm{T}} = 0.6 \cdot L$. Markers indicate the spatial responses from bandwidths of $1 \cdot \omega_{\mathrm{C}}$, $2 \cdot \omega_{\mathrm{C}}$, and $9 \cdot \omega_{\mathrm{C}}$ [reproduced from Fig. 4(c)]; responses from bandwidths of $3 \cdot \omega_{\mathrm{C}}$ and $4 \cdot \omega_{\mathrm{C}}$ (not marked) are sandwiched between the $2 \cdot \omega_{\mathrm{C}}$ and $9 \cdot \omega_{\mathrm{C}}$ response curves.

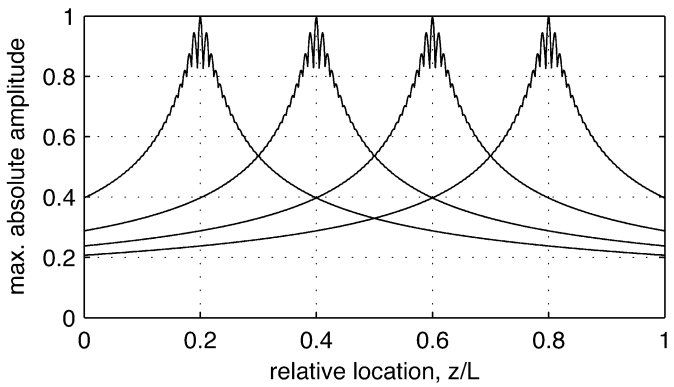

Fig. 6. Maximum absolute field intensity as a function of relative longitudinal distance. Data from $z_{\mathrm{T}} = 0.2, 0.4, 0.6$, and 0.8 m are superimposed and displayed the same as in Fig. 4(c). These results were obtained with $\omega_{\mathrm{MAX}} = 10 \cdot \omega_{\mathrm{C}}$ (bandwidth $\sim 9 \cdot \omega_{\mathrm{C}}$).

neglects phase interference, so that the actual signal decay is sharper than this bound.

The numeric simulation supports these theoretical results. In Fig. 6, the maximum points of constructive interference clearly occur at the intended targets, i.e., at $z_{\mathrm{T}} = [0.2, 0.4, 0.6, \mathrm{and} 0.8] \cdot L$. Further, the spatial decay

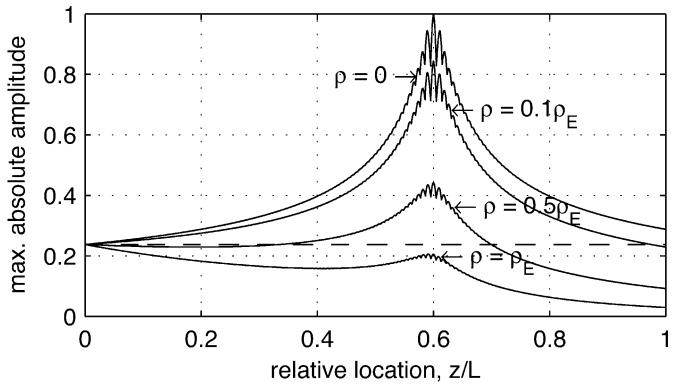

Fig. 7. Spatial results resulting from signal propagation in lossy media. Data from $\rho = [0, 0.1, 0.5, 1] \cdot \rho_E$ are superimposed and displayed the same as in Fig. 4(c). The spatial target was $z_{\mathrm{T}} = 0.6 \cdot L$. Markers indicate the spatial responses resulting from differing ρ [note that the case $\rho = 0$ is reproduced from Fig. 4(c)]. The dashed line represents the maximum field intensity of the signal at the input.

from the target matches the predicted upper bound of (42) and (43). Although these upper bounds neglect destructive phase interference, the gap between the bounds and the actual field intensity away from the target is small and consistent.

While these results demonstrate that dispersive systems can be exploited to achieve a spatio-temporal focus, it is not clear whether improved performance could be attained with a nonlinear signal construction. For example, more exact models of dispersive wave packets exist, especially for absorptive medium [20], [15], and it may be possible to construct a superior signal through such methods. In addition, techniques based on time-reversal or Fourier conjugate mirrors can effect the spatio-temporal matched filter in a scattering environment [21], [22], and as such may represent an alternate signal construction method. The asymptotic spatial decay of the presented approach is inversely proportional to the square root of distance from the target.

B. Waveguide Geometry for Optimal Performance

The analytic framework indicates an inverse relationship between spatial decay rate and the transverse dimension, A. Near the spatial target, spatial decay is bounded by $\sigma_1(z)$ in (21), which is inversely proportional to temporal capacity. According to (30), temporal capacity linearly increases with increasing distance from the target, with a slope of $2/(A\, W_\omega(3 + 2\sqrt{2}))$. While this slope is inversely proportional to W_ω, it is unlikely that major improvements can be attained by selecting from differing $\psi(t)$ functions. This is primarily due to results that state that the product of the variances of $\psi(t)$ and $\Psi(\omega)$ has a lower bound achievable only with a Gaussian envelope [17], [23]. However, the slope of the temporal capacity is also inversely proportional to A, the transverse dimension of the waveguide. Further, as was shown in the preceding section, at sufficient distances from the spatial target, the field is bounded by $\sigma_2(z) \propto \sqrt{A/|z_T - z|}$. Therefore, decreasing the transverse dimension will increase overall spatial decay.

While it may be possible to decrease the transverse dimension, this will affect the signal frequency range. For a fixed maximum velocity, decreasing the transverse dimension will increase the waveguide cutoff frequency and all parameters associated with it, because $\omega_{\mathrm{C}} = \nu_{\mathrm{M}}/A$. In particular, the optimal ω_{MAX} is $(\omega_{\mathrm{MAX}}/\omega_{\mathrm{C}})^2 \gg 1$; so the application bandwidth must also increase.[11]

However, it is incorrect to hold the theoretical maximum propagation velocity as sacrosanct. In homogeneous configurations, the theoretical maximum velocity of electromagnetic waves within a given medium is related to the permittivity (ϵ) and permeability (μ) of that medium

$$\nu_{\mathrm{M}} = \frac{1}{\sqrt{\mu\epsilon}}. \tag{45}$$

It is, therefore, possible to attain differing maximum velocities through materials with differing values of permittivity and permeability [25]–[27]. Dramatically different velocities may require special materials, such as in [28]. Also, "slow-wave" structures [29], acoustic waves in conjunction with piezoelectric materials [30], and ultraslowed group velocities brought about by electromagnetic induced transparency [31], [32], all produce lower propagation velocities. However, note that such configurations permit dispersion relations that are different from the relation assumed for this article. These relations can be exploited by following a similar signal construction to the presented construction.

Last, this work is not unrelated to the area of waveguide pulse-compression [33]. In that area, the waveguide signal is optimized to maximize output from the waveguide with certain restrictions on the waveguide input. As such, the properties of the signal *within* the waveguide are disregarded. Nevertheless, work in waveguide pulse-compression has produced structures and configurations that may be relevant to this work, including corrugated waveguides [34] and waveguides with periodic dielectrics [35].

V. Conclusion

The frequency-dependent velocity dispersion inherent to many waveguiding structures can be exploited to create a spatio-temporal focus at an arbitrary spatial target along the extent of the structure. This focus is dynamically-adjustable by applying a location-dependent linear filter to the waveguide input signal, which does not affect the underlying structure. The results scale with the physical parameters of the waveguiding structure, such that focused energy can be delivered to target locations within a variety of applications.

References

[1] S. Ramo, J. R. Whinnery, and T. Van Duzer, *Fields and Waves in Communication Electronics*, 3rd ed. New York: Wiley, 1994, pp. 398–402, 417–418.

[2] B. A. Auld, *Acoustic Fields and Waves in Solids*, 2nd ed. Malabar, FL: Robert E. Krieger, 1990, vol. 2, pp. 69ff–.

[3] W. Guo, J.-J. Xiao, and S. Cui, "An efficient water-filling solution for linear coherent joint estimation," *IEEE Trans. Signal Process.*, vol. 56, no. 10, pp. 5301–5305, 2008.

[4] A. G. Marques, X. Wang, and G. B. Giannakis, "Minimizing transmit power for coherent communications in wireless sensor networks with finite-rate feedback," *IEEE Trans. Signal Process.*, vol. 56, no. 9, pp. 4446–4457, 2008.

[11] Note, however, that some surface waveguides have $\omega_{\mathrm{C}} = 0$ [24].

[5] J. K. Tugnait, "On blind separation of convolutive mixtures of independent linear signals in unknown additive noise," *IEEE Trans. Signal Process.*, vol. 46, no. 11, pp. 3117–3123, 1998.
[6] J. K. Tugnait, "Parameter estimation for noncausal ARMA models of nongaussian signals via cumulant matching," *IEEE Trans. Signal Process.*, vol. 43, no. 4, pp. 886–893, 1995.
[7] J.-C. Hung and B.-S. Chen, "Genetic algorithm approach to fixed-order mixed h_2/h_∞ optimal deconvolution filter designs," *IEEE Trans. Signal Process.*, vol. 48, no. 12, pp. 3451–3461, 2000.
[8] D. S. Pham and A. M. Zoubir, "Estimation of multicomponent polynomial phase signals with missing observations," *IEEE Trans. Signal Process.*, vol. 56, no. 4, pp. 1710–1715, 2008.
[9] S. Oh, A. B. Milstein, R. P. Millane, C. A. Bouman, and K. J. Webb, "Source-detector calibration in three-dimensional Bayesian optical diffusion tomography," *J. Opt. Soc. Amer. A*, vol. 19, no. 10, pp. 1983–1993, 2002.
[10] J. B. Laflen, T. M. Talavage, and A. K. Sarychev, "High spatial resolution, focused electrical stimulation of electrically-excitable tissue," in *Proc. 2nd Joint Meet. IEEE EMBS and BMES*, Houston, TX, Oct. 2002, vol. 3, pp. 2080–2081, IEEE Eng. Med. Biol. Soc..
[11] J. B. Laflen, "measurement and analysis of perceptual coding in the human auditory system: Multi-modal studies using neural activation patterns," Ph.D. dissertation, Purdue Univ., West Lafayette, IN, Dec. 2003.
[12] J. B. Laflen and T. M. Talavage, "A theoretical, continuous alternative to the discrete electrode array," in *Cochlear Implants, ser. Int. Congress Series*. Indianapolis, IN: Elsevier, Nov. 2004, pp. 56–59, Vol. 1273.
[13] L. B. Felsen, *Transient Electromagnetic Fields*. Berlin, Germany: Springer-Verlag, 1976, pp. 31–38, ch. 1.4.5.
[14] K. A. Connor and L. B. Felsen, "Complex space-time rays and their application to pulse propagation in lossy dispersive media," *Proc. IEEE*, vol. 62, no. 11, pp. 1586–1598, 1974.
[15] E. Sonnenschein, I. Rutkevich, and D. Censor, "Wave packets, rays, and the role of real group velocity in absorbing media," *Phys. Rev. E*, vol. 57, no. 1, pp. 1005–1016, 1998.
[16] R. M. Lewis and J. B. Keller, Asymptotic methods for partial differential equations: The reduced wave equation and Maxwell's equations New York Univ., Courant Inst. Math. Sci., Div. Electromagn. Res., New York, Research Rep. 430681, Jan. 1964.
[17] S. Mallat, *A Wavelet Tour of Signal Processing*, 2nd ed. London, U.K.: Academic, 1999, pp. 30–33.
[18] D. Censor and J. J. Gavan, "Wave packets, group velocities, and rays in lossy media revisited," *IEEE Trans. Electromagn. Compat.*, vol. 31, no. 3, pp. 262–271, 1989.
[19] A. V. Oppenheim and A. S. Willsky, *Signals and Systems*. Upper Saddle River, NJ: Prentice-Hall, Pearson Education, 1997, pp. 422–, ch. 5.
[20] L. B. Felsen and N. Marcuvitz, *Radiation and Scattering of Waves*. Englewood Cliffs, NJ: Prentice-Hall, 1973, pp. 153–158, ch. 1.7e.
[21] J. M. F. Moura and Y. Jin, "Detection by time reversal: Single antenna," *IEEE Trans. Signal Process.*, vol. 55, no. 1, pp. 187–201, 2007.
[22] W. A. Kuperman, W. S. Hodgkiss, H. C. Song, T. Akal, C. Ferla, and D. R. Jackson, "Phase conjugation in the ocean: Experimental demonstration of an acoustic time-reversal mirror," *J. Acoust. Soc. Amer.*, vol. 103, no. 1, pp. 25–40, 1998.
[23] D. Gabor, "Theory of communication," *J. Inst. Elect. Eng.*, vol. 93, no. 26, pp. 429–457, 1946.
[24] R. E. Collin, *Field Theory of Guided Waves*. New York: McGraw-Hill, 1960, ch. 11.
[25] S. Ramo, J. R. Whinnery, and T. Van Duzer, *Fields and Waves in Communication Electronics*, 3rd ed. New York: Wiley, 1994, pp. 134–.
[26] L. D. Landau, E. M. Lifshitz, and L. P. Pitaevskii, *Electrodynamics of Continuous Media*, J. B. Sykes, J. S. Bell, and M. J. Kearsley, Eds., 2nd ed. Oxford: Butterworth-Heinemann, 1999, vol. 8, pp. 259–, Ser. Course of Theoretical Phys., translated from the Russian by.
[27] N. E. Hill, W. E. Vaughan, A. H. Price, and M. Davies, *Dielectric Properties and Molecular Behaviour*, ser. The Van Nostrand Series in Physical Chemistry. New York: Van Nostrand Reinhold, 1969, pp. 7–13.
[28] S. S. Bellad, S. C. Watawe, and B. K. Chougle, "Some AC electrical properties of Li-Mg ferrites," *Mater. Res. Bull.*, vol. 34, no. 7, pp. 1099–1106, 1999.
[29] S. Ramo, J. R. Whinnery, and T. Van Duzer, *Fields and Waves in Communication Electronics*, 3rd ed. New York: Wiley, 1994, pp. 476–478.
[30] B. A. Auld, *Acoustic Fields and Waves in Solids*, 2nd ed. Malabar, FL: Robert E. Krieger , 1990, Vol. 1 ch. 8.
[31] M. M. Kash *et al.*, "Ultraslow group velocity and enhanced nonlinear optical effects in a coherently driven hot atomic gas," *Phys. Rev. Lett.*, vol. 82, no. 26, pp. 5229–5232, Jun. 1999.
[32] C. Liu, Z. Dutton, C. H. Behroozi, and L. V. Hau, "Observation of coherent optical information storage in an atomic medium using halted light pulses," *Nature*, vol. 409, pp. 490–493, Jan. 2001.
[33] R. Bromley and B. Callan, "Use of a waveguide dispersive line in an f.m. pulse compression system," *Inst. Elect. Eng. Proc.*, vol. 114, no. 9, pp. 1213–1218, Sep. 1967.
[34] G. Burt, S. V. Samsonov, A. D. Phelps, K. R. Bratman, G. G. Denisov, W. He, A. R. Young, A. W. Cross, and I. V. Konoplev, "Microwave pulse compression using a helically corrugated waveguide," *IEEE Trans. Plasma Sci.*, vol. 33, no. 2, pp. 661–667, Apr. 2005.
[35] E. C. Thirios, D. I. Kaklamani, and N. K. Uzunoglu, "Microwave pulse compression using a periodically dielectric loaded dispersive waveguide section," *Electromagnetics*, vol. 26, pp. 345–358, 2006.

J. Brandon Laflen (M'01) received the B.S. degree and Ph.D. in electrical engineering from Purdue University, West Lafayette, IN, in 1998 and 2003.

He joined the faculty at New York University, New York, in 2005 and is affiliated with the Department of Otolaryngology, NYU Langone Medical Center.

Thomas M. Talavage (M'89) received the B.S. and M.S. degrees in electrical engineering from Purdue University, West Lafayette, IN, in 1992 and 1993, respectively, and the Ph.D. degree in speech and hearing sciences from the Harvard-MIT Division of Health Sciences and Technology, Cambridge, in 1998.

He joined the faculty of Purdue University in 1998, and is currently an Associate Professor with the School of Electrical and Computer Engineering and the Weldon School of Biomedical Engineering, Purdue University, and since 2007, has been Founding Co-Director of the Purdue MRI Facility, Weldon School of Biomedical Engineering.